



Single-photon counters in the telecom wavelength region of 1550 nm for quantum information processing

MOHAMED BOURENNANE, ANDERS KARLSSON,
JUAN PENA CISCAR and MARKUS MATHÈS

Department of Microelectronics and Information Technology,
Royal Institute of Technology (KTH), Electrum 229,
164 40 Kista, Sweden

(Received 29 January 2001; revision received 19 June 2001)

Abstract. We describe the status of commercially available InGaAs/InP avalanche photodiodes for use as single-photon counters in the telecom wavelength region of 1550 nm.

1. Introduction

Single-photon detection has become a useful technique in a wide range of fields in the last years. The photomultiplier tubes have been the detectors of choice in ultra-sensitive detection and spectroscopy [1]. Today, however, special semiconductor devices called single-photon avalanche diodes (SPADs or single-photon APDs) have been developed, and 'turn-key' modules for near-infrared, 600–900 nm photon counting. Silicon SPADs have very good performances: quantum efficiencies for detecting single-photons around 60%, dark counts, i.e. in the absence of light, is below 100 counts per second, and a sub-nanosecond timing resolution. Photon counting modules based on silicon SPADs are commercially available from EG&G Canada.

If one wishes to pursue photon counting at the longer telecom wavelengths of 1550 nm the situation is no longer that easy. Near-infrared photomultiplier tubes, such as Hamamatsu R5509-72, exist and have a spectral response up to 1700 nm, although with a quantum efficiency below the one percent level. The 0.73 eV band gap of the InGaAs lattice matched to InP allows single-photon sensitivity possibly up to a wavelength of 1700 nm. Few groups have therefore turned their attention to using commercially available InGaAs/InP APDs [2], originally developed for optical communication applications. In this work we have evaluated the performance of different InGaAs/InP APDs. This paper is organized as follows. In section 2, we discuss the SPAD's applications such as quantum communications, and in particular the quantum key distribution. In sections 3 and 4, we describe the basic principles of operation and the circuitry respectively. In section 5, we give our results for dark count probability P_{dark} , the noise-equivalent power (NEP), the ratio of P_{dark} and the quantum efficiency η , and the time resolution as a function of the temperature and the excess voltage. Then we present our single-photon counting module in section 6 and finally, in section 7, we draw some conclusions.

2. Applications

2.1. Quantum communications

In classical communications databits are encoded with a large number of photons per bit. However there is no fundamental reason why we cannot encode bits on individual photons. Under such conditions, quantum properties of the photons, like their particle-wave duality, become important. The emerging field of quantum communication tries to use quantum mechanics, such as the superposition principle, unitarity, the no-cloning theorem and quantum entanglement (which are quantum correlations that have no classical counterparts), for new forms of information processing. Many experimental realizations, such as quantum key distribution [3–7], quantum teleportation [8] and superdense coding [9], where the detection of single photons is crucial, have been demonstrated. One of the basic elements of quantum information processing is the interferometer. Let us describe, as an example, the Mach–Zehnder interferometer. Using the superposition principle of quantum mechanics, the initial state $|i\rangle$ undergoes the following sequence of transformations (see figure 1):

$$\begin{aligned}
 |i\rangle &\xrightarrow{\text{BS1}} \frac{1}{2^{1/2}}(|0\rangle + |1\rangle) \\
 &\xrightarrow{\Delta\phi} \frac{1}{2^{1/2}}(|0\rangle + \exp i\Delta\phi|1\rangle) \\
 &\xrightarrow{\text{BS2}} \cos\left(\frac{1}{2}\Delta\phi\right)|0\rangle + i \sin\left(\frac{1}{2}\Delta\phi\right)|1\rangle.
 \end{aligned} \tag{1}$$

The probability of counting in the detector D_1 is $P_1 = \cos^2\left(\frac{1}{2}\Delta\phi\right)$ and for detector D_2 it is $P_2 = \sin^2\left(\frac{1}{2}\Delta\phi\right)$.

The most advanced realization in terms of quantum information technology is quantum key distribution, where quantum mechanics provides a way to establish a

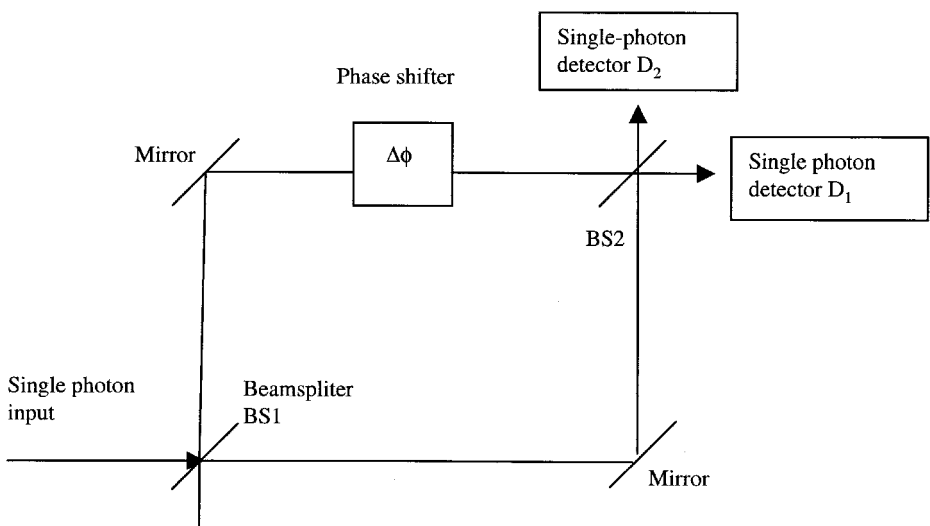


Figure 1. Mach–Zehnder interferometer with a phase shift between the upper and lower arms.

secret key between two remote parties. In general, the experimental set-up consists of two interferometers, one for the sender, Alice, and one for the receiver, Bob, and the bits sent by Alice are encoded on individual photons, using a similar arrangement such as the Mach-Zender interferometer presented above. To obtain some information, Bob has to perform a measurement on this single-photon state. However, according to quantum mechanics, a measurement disturbs the initial state sent by Alice. This fact allows the two users to reveal the presence of an eavesdropper by comparing their strings of bits. In the absence of noise these two strings must be identical. Clearly, if the detector noise is comparable to the noise introduced by a potential eavesdropper, Alice and Bob cannot detect the eavesdropper. Therefore, the detector noise must be negligible. To quantify this, we can define a quantum bit error rate (QBER) due to detector noise as

$$\text{QBER} = \frac{P_{\text{dark}}}{2P_{\text{dark}} + 10^{-\alpha L/10} \mu \eta}, \quad (2)$$

where for a 1550 nm system, the loss in the fibre is $\alpha = 0.2 \text{ dB km}^{-1}$ and $\mu = 0.1$ photons per pulse is used on average. If we want to have a system working up to a transmission distance of $L = 50 \text{ km}$ with an error rate lower than $\text{QBER} = 5\%$, we find that $P_{\text{eff}} = P_{\text{dark}}/\eta < 5.55 \times 10^{-4}$ is required. This is almost reachable with present InGaAs/InP SPADs.

2.2. Photon counting optical domain reflectometry

Optical time domain reflectometers (OTDRs) are very common tools used to characterize optical components and networks. A source emits light pulses coupled into the device under test. One records then the amount of light reflected as a function of time since the emission. If one knows the index of refraction of the system or the propagation velocity of the light pulses, it is possible to convert the time to distance. This principle makes it possible to perform distributed measurements of optical properties. Photon counting detectors, with their inherent sensitivity and timing resolution, are interesting solutions to extend the resolution of classical optical time domain reflectometry. What performance of photon counting OTDRs can be expected? Assuming that we could reach a 100 ps timing resolution in the time-of-flight information of the light pulse, this would correspond to a spatial resolution of about 1 cm in the optical fibre. An optical pulse of 200 mW power and of 100 ps pulse duration at the 1550 nm telecom wavelength contains about 2×10^8 photons. Assuming a 5% quantum efficiency and a dark count probability of $P_{\text{dark}} = 10^{-4}$ this implies that 110 dB of return losses can be sustained by the reflectometer before dark counts dominate the return! In a typical fibre of attenuation 0.2 dB km^{-1} this suggests sensitivity to -70 dB reflections at 100 km range with the signal-to-noise ratio = 10 from 100 pulses. This timing resolution and the suggested sensitivity would offer a substantial improvement over commercially standard OTDRs. Today, commercially available OTDR-based photon counting instruments are beginning to emerge.

3. The basic principles of operation

After having discussed the possible applications of the single-photon detector, let us now describe the basic principles of operation. An avalanche photodiode, or an APD for short, is basically a p-i-n diode specifically designed to provide an

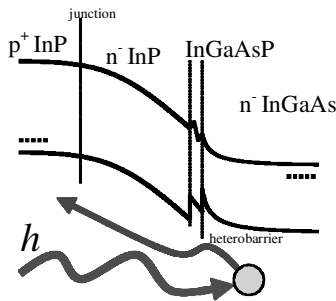


Figure 2. Schematic figure of the band diagram of the separate absorption and multiplication region in an InGaAs APD.

internal current gain, making it much more sensitive to small light fluxes. The physical phenomenon behind the current gain is known as impact ionization. When reverse biased, the APD is designed to be able to sustain a large electric field across the intrinsic *i*-region between the *p*-type layer and the *n*-type layer, as seen in the schematic band diagram of figure 2. An incoming photon is absorbed to create an electron–hole pair in the narrow bandgap InGaAs *i*-layer. The generated hole crosses to the wider bandgap InP multiplication region, which due to the doping sustains most of the electric field, and where the hole is accelerated to gain enough energy to generate secondary electron–hole pairs by impact ionization. These in turn can generate new electron–hole pairs, and so forth. Generally, the generation rate of electrons and holes is governed by two parameters α_e and α_h , called the impact-ionization parameters of electrons and holes, respectively. The APDs are classified by their internal electric field profile and by the layer structure. Practically, the performance of the APD is better when only one carrier type contributes to the multiplication process. For silicon, the ratio of the electron and the hole ionization coefficient is about 100:1 for an electric field of 200 kV cm^{-1} , and silicon APDs are designed to have multiplication by electrons in a *p*-doped multiplication region. For InP at the same electric fields, the ratio is inverse and is only about 1:4. Therefore holes initiate the multiplication process in an *n*-doped multiplication region. The reasons for a InP multiplication region instead of an InGaAs region is that the hole and electron impact-ionization coefficients are comparable for InGaAs; also in the narrow InGaAs region tunnelling breakdown may occur for fields lower than the threshold for avalanche multiplication. Because of the band-gap difference between the InGaAs and the InP there will be a step in the valence band, which may trap the holes and slow down the response. A grading with a quaternary InGaAsP layer is therefore used to smooth the discontinuity. The resulting avalanche process will cause large currents to flow through the device, and special device structures are needed to tolerate the high bias condition without breaking down due to bulk or surface effects. For conventional optical communication applications, the reverse voltage applied is below the so-called breakdown voltage V_B , the point at which thermal fluctuations or tunnelling will initiate the avalanche process by themselves. Below the breakdown regime the output remains a linearly amplified copy of the input signal. Commercially available InGaAs APDs, such as EG&G C306444EJT-07 and NEC NDL5551PC are all designed with the linear regime, and as we will discuss

later, this regime is not necessarily well adapted to the requirements for single-photon counting. To achieve single-photon sensitivity in the detection, the SPADs are biased in a so-called ‘Geiger mode’, with an excess bias voltage V_E above the breakdown voltage. In this case, the amplification effectively becomes infinite and even a single-photon absorption causes an avalanche with a macroscopic current pulse which can readily be detected by ensuing electrical circuitry. This circuitry must also suppress the avalanche process before it actually destroys the device. The value of the breakdown voltage V_B is structure, material and temperature dependent and may range from 10 to 500 V. For optical communication InGaAs/InP APDs it is typically around 50 V. Raising the bias voltage V_E increases the quantum efficiency, but also increases the dark count noise. What matters for the performance is the excess electrical field across the devices, which is related to the ratio V_E/V_B . Typical values used for V_E are in the range of one to a few volts.

4. Circuits for single-photon counting

When an avalanche is triggered, either by a photon or a noise event, a current starts to flow in the device and rapidly reaches the milli-ampere range. One must connect proper electronics to the detector to sense the current and quench the avalanche in order to avoid damaging the device. After a time interval long enough for the photodiode to recover, the excess bias voltage is raised again above breakdown to reactivate the detector. There are several ways to realize the quenching and the Milan group [10, 11] has done detailed studies on the performance of SPADs with various quenching circuits. Let us describe in detail the circuit which we have used. This combines the two following circuits: gated and passive quenching circuits.

4.1. *Passive quenching circuit*

For passive quenching circuit (PQC), the APD is placed in series with a large load resistor in the tens of $k\Omega$ range to drop down the diode voltage below V_B after the avalanche has been triggered. The voltage across the diode is then slowly restored to the bias voltage through the natural dead-time associated with the time taken to recharge the SPAD capacitance via the load resistor. In order to obtain an output pulse from a PQC SPAD, one typically inserts a low-value series resistor R_s on the ground lead of the circuit. A convenient value is $R_s = 50 \Omega$, since it provides matched termination for a coaxial cable that can be directly connected to the APD terminal. With R_s on the ground lead of the diode the waveform of the pulse is directly that of the diode current and this mode of operation is therefore called current mode output. This mode offers the best performance in high rate counting and in precision pulse timing, and is usually preferred. A PQC does not allow a very high excess bias which, as we will see, puts some restrictions on the quantum efficiency and timing resolution one can reach. Furthermore, PQC does not seem to work very well with InGaAs SPADs.

4.2. *Gated passive quenching circuit*

In many applications, the arrival time of the photon at the junction is known, or can be scanned for, making it possible to use a gated mode of operation. In this approach the APD bias voltage is brought above breakdown for short time periods, T_w , during which avalanche may occur. The order of magnitude for T_w is typically

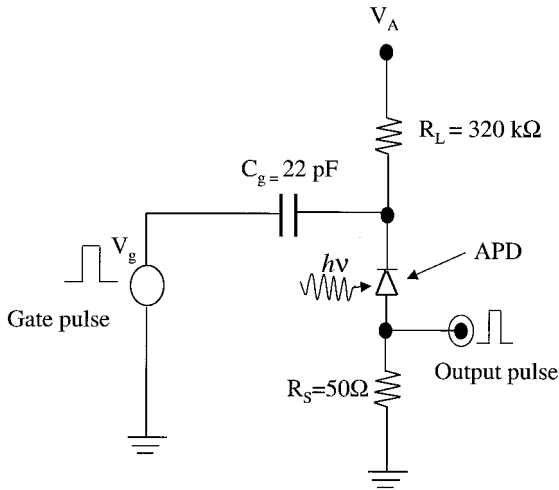


Figure 3. Schematic circuit diagram of the gated passive quenching circuit.

around a few nanoseconds. These periods are separated by a longer hold off time, T_h , when the bias voltage is brought below the breakdown level. The gating pulse can simply be added directly in series to the dc bias voltage V_A .

We have combined passive quenching with gating, as shown schematically in figure 3. Thanks to the possibility of applying a high excess voltage bias, this technique makes it possible to achieve high detection efficiency and good timing resolution. In addition, the fact that the detector is activated only for a short time interval allows the noise to be reduced. With present day SPADs, this technique should be used every time one can predict precisely the time of arrival of the photons.

5. Detector characterization and performance

As a designer of SPAD circuits based on commercial SPADs, there are basically two parameters one can control for optimizing the SPAD performance: the device operating temperature T and the excess bias voltage V_E (or the gate voltage). Let us therefore now discuss how these parameters affect the performance.

5.1. Detector characterization experimental set-up

To control the temperature, the APD is placed in a closed box, which is immersed in liquid nitrogen, and the temperature is adjusted through electrical heating. With the help of a temperature controller, we can measure with an accuracy of ± 1 degrees. The APD is operated in a gated mode, lifting the biased voltage above the breakdown voltage for 3.5 ns, when we expect a signal to arrive. A passive quenching circuit with a 320 kΩ series resistance providing the dc bias was used. The output signal was measured over a 50 Ω load resistance [12, 13].

5.2. Dark counting

The avalanche rate in SPADs is due not only to signal photons but may also be randomly triggered by bulk carriers generated in thermal, tunnelling or trapping

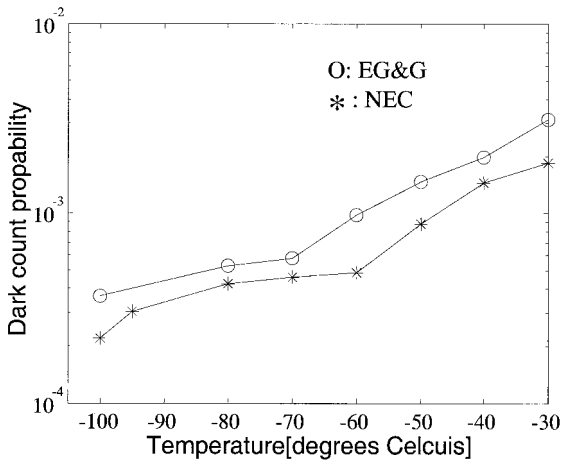


Figure 4. Dark count probability as a function of the temperature and fixed voltage for the EG&G and NEC APDs.

processes inside the semiconductor. These processes cause a self-triggering rate of the detector that is called the dark counting rate, R_{dark} . Typically, R_{dark} in silicon SPADs are about ten to one hundred counts per second, whereas for InGaAs/InP SPADs having more random bulk carriers, R_{dark} is in the order of hundreds of thousands of counts per second. In the gating mode, we measure the dark count probability per gate pulse P_{dark} . If we make the assumption that the dark counts occur uniformly within the gate window, then the probability of a dark count per gate pulse simply becomes

$$P_{\text{dark}} = R_{\text{dark}} T_w, \quad (3)$$

where T_w is the width of the gate pulse.

The easiest way to reduce the effect of dark counts is to cool the detector. This reduces the effect of thermal noise. However, beyond a certain range it is not worth going further down in temperature since the tunnelling effect dominates at low temperatures, and it is weakly dependent on temperature. Also, the quantum efficiency decreases with decreasing temperature, so there will be an optimum operating point. An equally important parameter is the device's excess bias voltage V_E . The device's quantum efficiency increases with excess bias voltage, but so does the noise. In the figure 4 we plot P_{dark} , the dark count probability per gate pulse, versus the temperature for EG&G C306444EJT-07 and NEC NDL5551PC; we observe that the NEC APD is less noisy than the EG&G APD. In figure 5 we plot the P_{dark} versus the gate voltage for three different temperatures $T = -80^\circ\text{C}$, -70°C and -60°C for NEC NDL5551PC. We observe that P_{dark} increases when the gate voltage increases.

5.3. Afterpulsing

Perhaps the major plague of InGaAs/InP SPADs to date is due to so-called afterpulses enhancing R_{dark} . Afterpulses arise from trapping centres due to minority carrier trapped in the high field region of the junction where impact ionization occurs. Most afterpulses occur within microseconds of the initial pulse. The afterpulses are proportional to the number of filled traps, which in turn are

proportional to the charge that passes through the device before quenching takes place. The larger the charge flowing through the device the higher the number of carriers trapped and the more recurrent the afterpulses. Since charge is proportional to capacitance times voltage, the afterpulsing fraction increases with excess bias, V_E . To minimize the trapping enhancement of R_{dark} , the condition of operation of the device must be chosen so as to reduce the trapping of the carriers and to decrease the release time of the trapped carriers. The emission lifetime of the carriers from trapping levels unfortunately increases exponentially with a reduction in temperature. So far the cure to get rid of the dark count rate enhancement due to trapping effects has been to use a gated detection scheme. If the APD has been gated for a sufficiently long time interval, longer than the trap release time, before bringing it back into operation, trap levels are almost all empty and do not trigger any avalanche. We have worked at 1 kHz repetition rate, which is very large compared to the inverse of a typical trapping time (microseconds regime), therefore the afterpulses are negligible. Rarity *et al.* [14] have analysed the afterpulse effects by measuring the photocount autocorrelation and using a passive quenching circuit. They found that the afterpulse probability increases with the photon electron detection efficiency and decreases with delay time (time interval between the detection photon pulse and the laser timing pulse).

5.4. Quantum efficiency

The quantum efficiency η in the Geiger mode results from three factors:

- (1) the probability that a photon will be absorbed in the InGaAs layer—absorption efficiency;
- (2) the probability that the photon generated carriers will trigger the avalanche when crossing the junction—trigger probability (increases with the excess bias V_E above V_B);
- (3) the optical coupling efficiency of the light to the device.

When the temperature increases, the APD's quantum efficiency increases to reach a maximum and then starts to decrease again. In figure 6, we plot the quantum

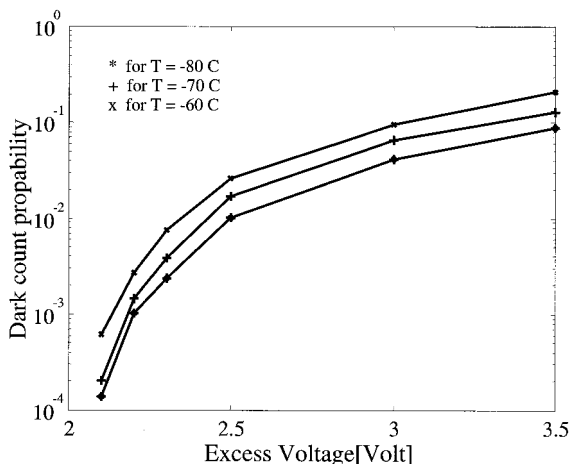


Figure 5. Dark count probability as a function of the excess voltage and for three fixed temperatures, $T = -80^\circ\text{C}$, -70°C and -60°C , for an APD from NEC.

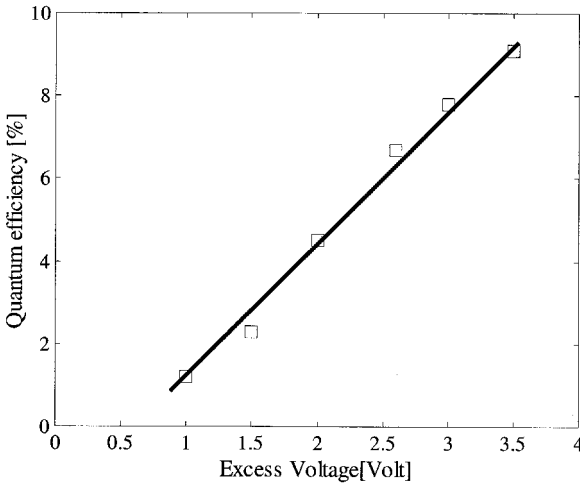


Figure 6. The quantum efficiency as a function of the excess voltage for fixed temperature, $T = -110^{\circ}\text{C}$, for an APD from NEC.

efficiency as a function of the excess voltage for fixed temperature, and we see that the quantum efficiency increases with the excess bias voltage. But as we observe in figure 4, the noise increases too. Therefore we need to find a trade-off between increasing the quantum efficiency and decreasing the dark counting probability, and to find an optimum operating temperature and gate voltage.

6. Figure of merits

Since both the quantum efficiency, η , and the dark count rate, P_{dark} , contribute to the detector sensitivity, one would need a figure-of-merit taking both into account. In optical communications, the benchmark used is the NEP, which is defined as the signal power required to attain a unity signal-to-noise ratio within 1 s integration time, giving by

$$\text{NEP} = \frac{h\nu}{\eta} (2R_{\text{dark}})^{1/2} = \frac{h\nu}{\eta} \left(\frac{2P_{\text{dark}}}{T_w} \right)^{1/2}, \quad (4)$$

where $h\nu$ is the photon energy. In figure 7, we present the NEP, for EG&G InGaAs C306444EJT and NEC NDL5551PC APDs as a function of temperature; the curves have a minimum, which corresponds to the maximum of the quantum efficiency. It is important to note that the optimum of NEP occurs at about -60°C and -150°C for EG&G and NEC respectively. These temperatures can be reached by Peltier cooling. For single-photon counting applications, it should be stressed that the NEP is not necessarily the most useful quantity. As we have seen in section 2.1, what rather counts is, given that a single-photon arrives at the detector, the probability of having a count from the photon compared to the probability for having a false count caused by dark counts. The benchmark to use would be the dark count probability per counted photon assuming one photon incident per gate pulse, which can be written as

$$P_{\text{eff}} = \frac{P_{\text{dark}}}{\eta}. \quad (5)$$

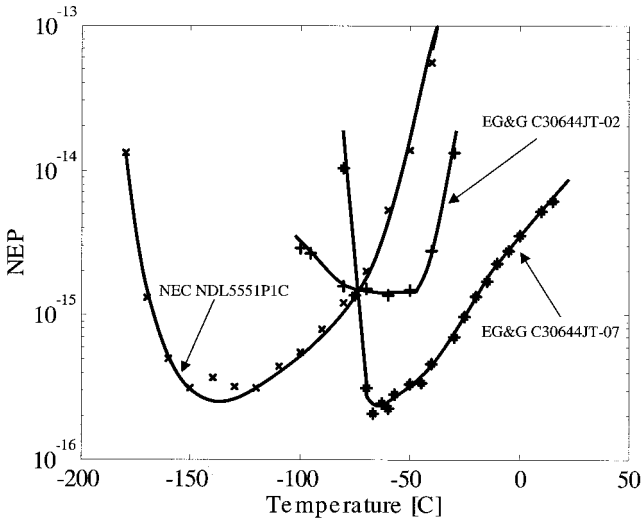


Figure 7. The noise-equivalent power (NEP) as a function of the temperature and fixed excess voltage for different APDs.

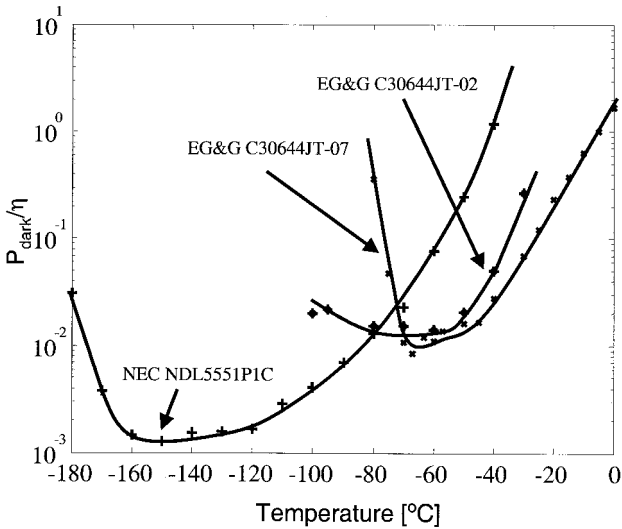


Figure 8. The ratio of the dark count probability and the quantum efficiency as a function of the temperature and fixed excess voltage for different APDs.

In figure 8, the P_{eff} for EG&G InGaAs C306444EJT and NEC NDL5551PC APDs are shown. Comparing to the NEP, since the dependence on P_{dark} is different, the optimum performance now should be reached at a different temperature and excess bias voltage. In practice there is no large difference. We observe that the optimum of P_{eff} occurs at about -150° and -60°C for the NEC and EG&G APDs respectively. For applications in telecom, $T = -60^\circ\text{C}$ can be reached with Peltier cooling.

6.1. Timing resolution

For many applications the timing resolution of the detection is important. In a simple picture, the timing resolution depends on how fast the photogenerated carriers can be swept out from the absorption region. The timing resolution is understood as the response jitter of the APD to the arrival photon. The APD's response is a curve with a maximum, and the FWHM (full width half maximum) of this curve is called the timing resolution. The output pulses from APD are sensed by the single-photon counting card which essentially is the time-to-amplitude converter (TAC). The gate pulse is used to start the reference pulse. We have used a SPC 300 card from PicoQuant. In figure 9, we plot the timing resolution versus the gate pulse and we observe that the timing performance improves with an increased excess bias. We obtain timing resolutions down to 200 ps for high gate voltage, which is the situation when the dark count probability is also high. In table 1, we compare the timing resolution for different APDs. We see that the timing resolution of InGaAs/InP APDs are higher than the silica APDs. For the InGaAs/InP EG&G APDs, our timing resolutions are lower compared to the results obtained in [16] for Fujitsu APDs.

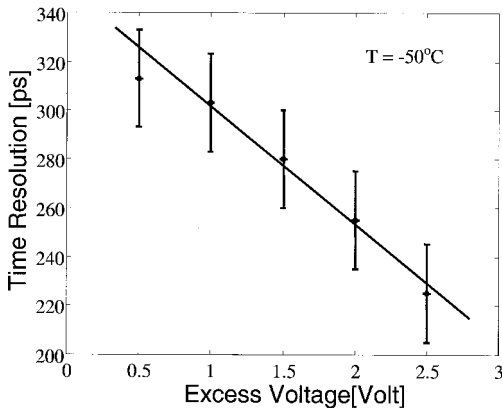


Figure 9. Time resolution as a function of the excess voltage for fixed temperature, $T = -50^{\circ}\text{C}$, for an APD from EG&G.

Table 1. Comparison of the timing resolution for different APDs.

Group	Detector	Material	Wavelength	Temperature and excess voltage	Timing resolution
KTH	EG&G	InGaAs/InP	1.55 μm	298 K & 0.5 V	302 ps
KTH	EG&G	InGaAs/InP	1.55 μm	289 K & 2.5 K	220 ps
Zappa <i>et al.</i> [15]	Fujitsui	InGaAs/InP	1.3 μm	150 K	450 ps
Hiskett <i>et al.</i> [16]	Fujitsu	InGaAs/InP	1.5 μm	77 K & 1 V	253 ps
Ribordy <i>et al.</i> [12]	Fujitsu	InGaAs/InP	1.3 μm	173 K	180 ps
Zappa <i>et al.</i> [15]	EG&G/RCA C30902S	Silica	840 nm	—	320 ps
Zappa <i>et al.</i> [15]	EG&G SLIK	Silica	840 nm	—	168 ps

7. Single-photon counter module

After the characterization of these APDs, the optimal parameter value has been found for the ratio of dark count probability and quantum efficiency. We have built a single-photon counter module working in these optimal conditions. These modules consist of an APD, 4-stages of Peltier cooling, gated passive quenching, fast discrimination, and conversion to TTL signal circuits. In figure 10, we show a photograph of our module; we are currently building more compact versions of the modules. In figure 11, we show the TTL signal output from our module. These signals can easily be sent to a computer for forward processing.



Figure 10. A photograph of our single-photon counter module (SPCM) with Peltier element cooling and a TTL signal output.

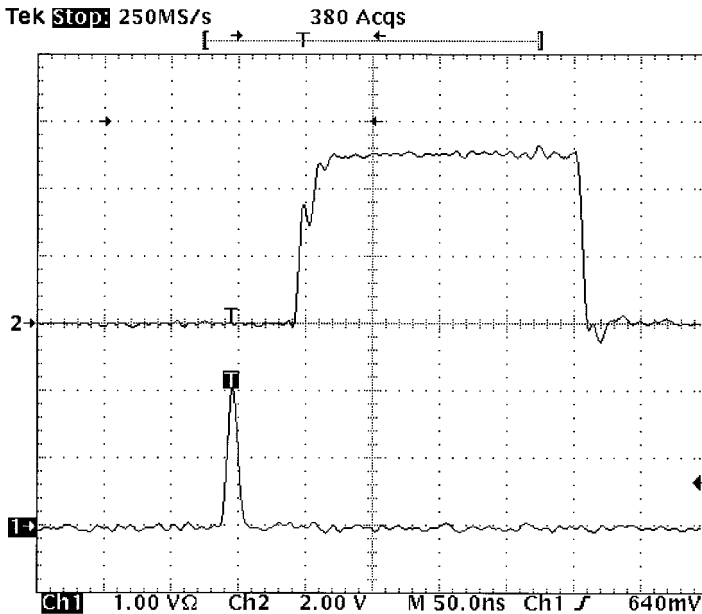


Figure 11. TTL output from our single-photon counter module.

8. Conclusion

In these studies, we have shown that the commercially available InGaAs/InP APDs can be used for single-photon counting. We have measured the dark count probability, quantum efficiency, noise-equivalent power, and the timing resolution of the APDs for different temperatures and gate voltages. These APDs come from different manufactures, and we observed, as other research groups, that their performance depends on the manufacturers and samples. We like to stress that for single-photon applications these APDs should be selected from a large sample batch. We have also built single-photon counting modules. In the future, we would like to study other APDs from other manufacturers and compare their performances. As seen in other contributions in this issue, improved results have been obtained [17].

Acknowledgments

This work was supported by The Swedish Technical Science Research Council (TFR) and the European Commission through the IST FET QIPC QuComm project.

References

- [1] O'CONNOR, V., and PHILLIPS, D., 1984, *Time-Correlated Single-Photon Counting Techniques* (London: Academic Press).
- [2] KARLSSON, A., BOURENNANE, M., RIBORDY, G., GAUTIER, J.-D., ZBINDEN, H., RARITY, J. G., and TAPSTER, P. D., 1999, *IEEE Circuits Devices Mag.*, **15**, 34.
- [3] RIBORDY, G., GAUTIER, J.-D., GISIN, N., GUINNARD, O., and ZBINDEN, H., 2000, *J. mod. Optics*, **47**, 517.
- [4] TOWNSEND, P. D., 1998, *Opt. fiber Technol.*, **4**, 345.
- [5] HUGHES, R., MORGAN, G., and PETERSON, C. G., 2000, *J. mod. Optics*, **47**, 533.
- [6] BOURENNANE, M., LJUNGGREN, D., KARLSSON, A., JONSSON, P., HENING, A., and CISCAR, J. P., 1999, *J. mod. Optics*, **47**, 563.
- [7] BETHUNE, D. S., and RISK, W. P., 2000, *IEEE J. quantum Electron.*, **36**, 340.
- [8] BOUWMEESTER, D., PAN, J.-W., MATTLE, K., EIBL, M., WEINFURTER, H., and ZEILINGER, A., 1997, *Nature*, **390**, 575.
- [9] MATTLE, K., KWIAT, P. G., WEINFURTER, H., and ZEILINGER, A., 1994, *Phys. Rev. Lett.*, **76**, 4656.
- [10] LACAITA, A., ZAPPA, F., COVA, S., and LOVATI, P., 1996, *Appl. Optics*, **35**, 2986.
- [11] COVA, S., GHIONI, M., LACAITA, A., SAMORI, C., and ZAPPA, F., 1996, *Appl. Optics*, **35**, 1956.
- [12] RIBORDY, G., GAUTIER, J.-D., ZBINDEN, H., and GISIN, N., 1998, *Appl. Optics*, **37**, 2272.
- [13] BOURENNANE, M., GIBSON, F., HENING, A., KARLSSON, A., JONSSON, P., TSEGAYE, T., LJUNGGREN, D., and SUNDBERG, E., 1999, *Optics Express*, **10**, 383.
- [14] RARITY, J. G., WALL, T. W., RIDLEY, K. D., OWENS, C. M. P., and TAPSTER, P. R., 2000, *Appl. Optics*, **39**, 6746.
- [15] ZAPPA, F., LACAITA, A. L., COVA, S. D., and LOVATI, P., 1996, *Opt. Eng.*, **35**, 1956.
- [16] HISKETT, P. A., BULLER, G. S., LOUDON, A. Y., SMITH, J. M., GONTIJO, I., WALKER, A. C., TOWNSEND, P. D., and ROBERTSON, 2000, *Appl. Optics*, **39**, 6818.
- [17] STUCKI, D., RIBORDY, G., STEFANOV, A., ZBINDEN, H., RARITY, J. G., and WALL, T., *J. mod. Optics*, this issue.